Circumventing Physicochemical Barriers of Cyclometalated Gold(III) Dithiocarbamate Complexes with Protein-Based Nanoparticle Delivery to Enhance Anticancer Activity

Adedamola S. Arojojoye, Breyanna Walker, James C. Dawahare, Maame Abena O. Afrifa, Sean Parkin, and Samuel G. Awuah*

Cite This: https://doi.org/10.1021/acsami.3c10025

Read Online

ACCESS | Metrics & More | Article Recommendations | Supporting Information

ABSTRACT: Optimizing the bioavailability of drug candidates is crucial to successful drug development campaigns, especially for metal-derived chemotherapeutic agents. Nanoparticle delivery strategies can be deployed to overcome physicochemical limitations associated with drugs to improve bioavailability, pharmacokinetics, efficacy, and minimize toxicity. Biodegradable albumin nanoconstructs offer pragmatic solutions for drug delivery of metallodrugs with translational benefits in the clinic. In this work, we explored a logical approach to investigate and resolve the physicochemical drawbacks of gold(III) complexes with albumin nanoparticle delivery to improve solubility, enhance intracellular accumulation, circumvent premature deactivation, and enhance anticancer activity. We synthesized and characterized stable gold(III) dithiocarbamate complexes with a variable degree of cyclometalation such as phenylpyridine (C^N) or biphenyl (C^C) Au(III) framework and different alkyl chain lengths. We noted that extended alkyl chain lengths impaired the solubility of these complexes in biological media, thus adversely impacting potency. Encapsulation of these complexes in bovine serum albumin (BSA) reversed solubility limitations and improved cancer cytotoxicity by ~25-fold. Further speciation and mechanism of action studies demonstrate the stability of the compounds and alteration of mitochondria bioenergetics, respectively. We postulate that this nanodelivery strategy is a relevant approach for translational small-molecule gold drug delivery.

KEYWORDS: gold(III), dithiocarbamate, nanoparticles, bovine serum albumin, encapsulation, stability, cyclometalation
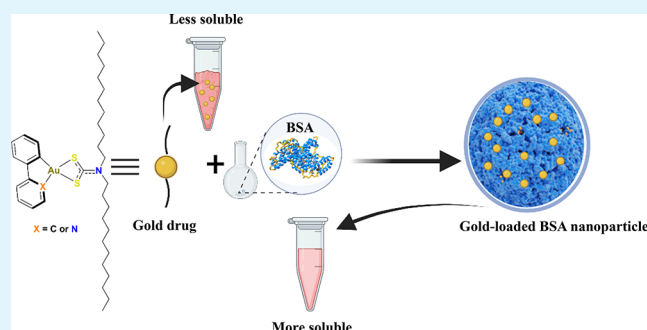
INTRODUCTION

Despite the significant progress in the development of novel chemotherapeutic agents in the past few decades, cancer remains a leading cause of death in the United States.[1-5] Different approaches have been employed in the development of novel chemotherapeutics with metallodrugs playing a prominent role since the approval of cisplatin, oxaliplatin, and carboplatin for the treatment of testicular, colon, and ovarian cancer.[6-11] Metal complexes possess unique properties such as multiple oxidation states, unique redox potential, and geometry that make them desirable chemotherapeutics.[1,12-16] Despite these desirable qualities, research into metal-based drugs suffers a number of setbacks due to physicochemical and physiological factors such as off-target effects, poor stability, aggregation, degradation, and poor cellular uptake; which have stalled their progression to the clinic.[17,18] These factors correlate with pharmacokinetic properties, which are defined by the absorption, distribution, metabolism, and excretion (ADME) properties of a potential drug molecule.[11] Although these can be modeled by examining the octanol/water partition coefficient or the Lipinski rule for lipophilicity that has proved useful in many organic-based drug discovery efforts, there is a need for caution when metallodrugs are involved.[19,20] On the issue of stability of metal-based complexes, cyclometalation is an attractive method.[21] Here, the metal is stabilized or chelated by a carboligand, this chelation confers improved stability to the highly susceptible metal–carbon bond giving metallodrugs increased stability.[22] Also, to modulate the physicochemical properties, increasing the alkyl chain length could improve the lipophilicity due to the tendency for longer chains to fill binding pocket of protein, increase hydrophobic interactions between the compound, and the target thus imparting cellular response.[23,24]
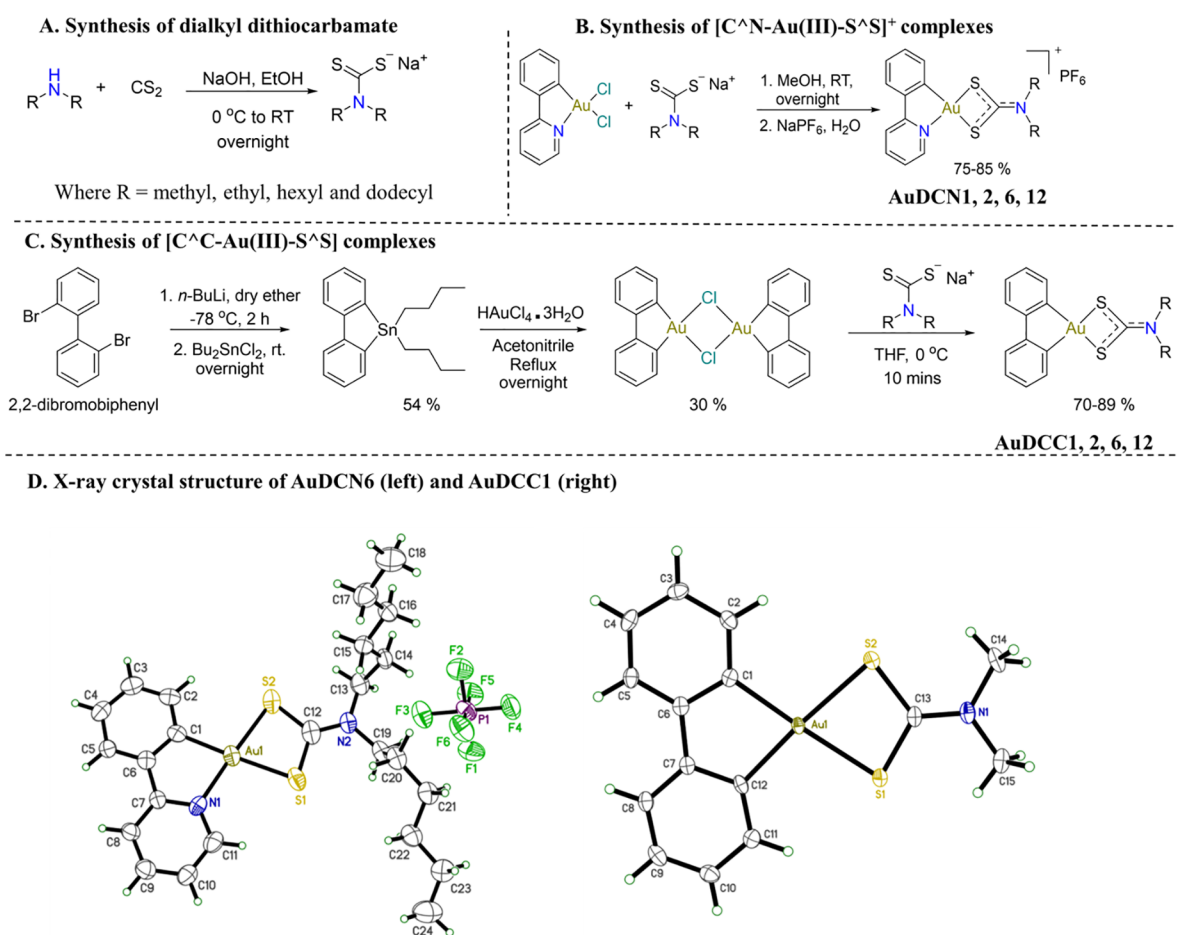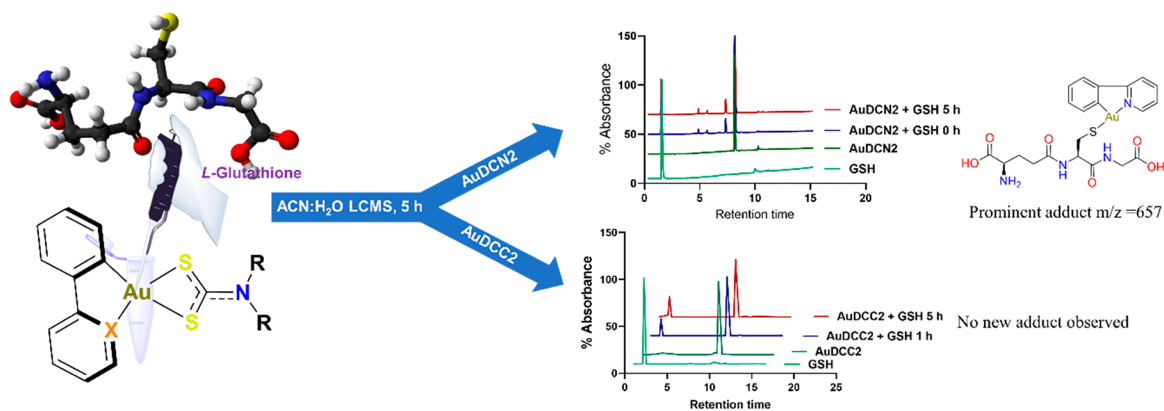
Figure 1. Synthetic scheme to access cyclometalated gold(III) dithiocarbamate. (A) Synthesis of dialkyldithiocarbamate. (B) Synthesis of cationic [C^N-Au(III)-S^S]PF$_6$ complexes. (C) Synthesis of neutral [C^C-Au(III)-S^S] D) X-ray crystal structures of **AuDCN6** and **AuDCC1** complexes. Thermal ellipsoids are shown at the 50% probability level.

Encapsulating metallodrugs with natural biocompatible proteins such as albumin can further improve solubility and absorption of metallodrugs into cells.[25,26] Albumin is an abundant protein in blood that binds ligands and facilitates transport within cells. Albumin accumulates preferentially in leaky vessels, where they are readily internalized by nutrient deprived cancer cells. Also, albumin encapsulated drugs have shown low toxicity with a long plasma circulation half-life.[27−29] In addition to these characteristics, the rationale that cancer cells overexpress albumin receptors such as neonatal Fc receptor (FcRn), glycoprotein (gp60, gp30, gp18) receptors where it activates caveolin-1 to mediate the transcytosis of albumin-bound molecules and Secreted Protein Acidic Rich in Cysteine (SPARC) receptor that modulates extracellular proliferation and cell migration associated with increased tumor invasion has made encapsulation with albumin an attractive option in drug delivery systems.[30−34] Abraxane a notable albumin-based drug approved by the FDA is used for patients with metastatic breast cancer, non-small cell lung cancer, and pancreatic adenocarcinoma.[27,35,36] Other albumin encapsulated drugs such as nab-5404 (NCT01163071) and nab-docetaxel (NCT00477529) which are based on the albumin bound technology (nabtechnology) similar to Abraxane are currently undergoing clinical trials.

Research into the use of albumin as a carrier for transition-metal-based complexes is promising. BTP-114, an albumin binding platinum prodrug is currently undergoing clinical trial for treating patients with advanced solid tumors with BRCA mutations (NCT02950064) and reports of other platinum, palladium, and copper loaded albumin systems are present in the current literature.[25,31,37−43] In recent years, research into gold(III) complexes has increased with the aim of overcoming drug resistance and deleterious side effects associated with platinum-based drugs, unravel newer mechanism of drug action, and identify molecular targets.[44−52] Hence, we explored the use of bovine serum albumin (BSA) as a carrier for gold(III) dithiocarbamate complexes. Albumin loaded gold-(III)-dithiocarbamate complexes are attractive as results from preclinical evaluation of peptidomimetic delivered gold(III)-dithiocarbamate complexes showed excellent antineoplastic activity in cisplatin resistant cells,[53,54] but their premature deactivation has limited their progression to the clinic. Herein, we investigate the effect of gold(III) dithiocarbamate complexes with different degrees of cyclometalation and alkyl chain length on cellular responses in cancer cell lines. To overcome the solubility problems inherent in longer chain gold(III) dithiocarbamate, we encapsulated dodecyl dithiocarbamate Au(III) complexes in BSA to form nanoconstructs and further characterized their biological responses in cancer cells.
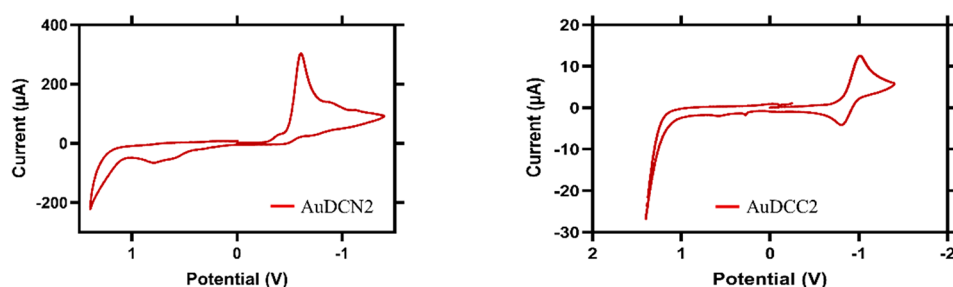
Figure 2. Stability Studies of Au(III) dithiocarbamate complexes. (A) Chart showing the reaction of **AuDCN2** and **AuDCC2** with L-GSH monitored by LCMS. HPLC conditions Flow rate: 1 mL/min; λ = 260 nm; Eluent A = DI. water with 0.1% trifluoroacetic acid; Eluent B = Acetonitrile with 0.05% formic acid; Solvent Gradient: 0−16 min (0:100 H_2O: ACN). Sixteen min until end of run (100:0 H_2O: ACN). (B) Cyclic voltammetry studies of **AuDCN2** (5 mM) and **AuDCC2** (5 mM) in DMSO with 0.1 M NBu_4PF_6 as the supporting electrolyte at a platinum electrode with a Ag/AgCl reference electrode. Scan rate = 0.1 V/s; Quiet time = 2 s; sensitivity = 1 × 10^{-5} A/V.

■ RESULT AND DISCUSSION

Synthesis. In this work, we report the synthesis of gold(III) dithiocarbamate complexes using two different organogold(III) starting materials bearing [C^N] and [C^C] cyclometalated gold(III) framework and explored the impact of different cyclometalation approaches on the cellular response in cancer cells. The two scaffolds differ only in Au−N and Au−C bonds. The synthetic scheme proceeds by reacting an ethanolic solution of dialkylamine with carbon disulfide to afford dialkyldithiocarbamate with varying alkyl chain lengths 1, 2, 6, and 12 (Figure 1A). This was followed by the synthesis of either the C^N or C^C cyclometalated gold(III) complexes. Subsequently, **AuDCN1**, **2**, **6**, and **12** were synthesized by reacting a methanolic solution of dichloro(2-phenylpyridine)-gold(III) with the corresponding dialkyldithiocarbamate at room temperature to give cationic gold(III) complexes of the type [C^N-Au(III)-S^S]$^+$ (Figure 1B). To access the C^C cyclometalated complexes, we proceeded by synthesizing di-μ-chlorido biphenyl digold(III) via an already reported protocol,[55,56] this was then followed by the addition of dialkyldithiocarbamate in tetrahydrofuran to afford neutral gold(III) complexes **AuDCC1**, **2**, **6**, and **12** of the archetype [C^C-Au(III)-S^S] (Figure 1C). The compounds were fully characterized by NMR spectroscopy, and purity was assessed by HPLC-MS and found to be greater than 97% (Figures S1−S48). X-ray crystallography studies reveal that **AuDCN6** and **AuDCC1** have square planar geometry around the central gold atom. While **AuDCN6** crystallizes as a monocationic complex in a tetragonal $P\bar{4}2(1)c$ space group, **AuDCC1** crystallizes as a

neutral monoclinic gold(III) complex with a $P2(1)/n$ space group (Figure 1D), Tables S1−S2.

Stability and Speciation Studies. To understand the impact of the degree of cyclometalation on the stability of gold complexes, we carried out speciation studies. **AuDCN2** and **AuDCC2** were reacted with L-glutathione and monitored by LC-MS for 5 h to observe potential adduct formation. L-Glutathione is a major nonprotein thiol in cells where it exists in the reduced form at a concentration of about 10 mM and can readily react with electrophiles or reduce Lewis acids. Analysis of the HPLC trace of the reaction of **AuDCN2** or **AuDCC2** with L-GSH showed that both complexes were present in the reaction after 5 h (Figure 2A). However, a new peak was observed immediately after addition of L-GSH to **AuDCN2** complex which corresponds to the reduced [2-phenylpyridine-Au-GSH] adduct (m/z = 657) and this adduct decreased minimally during the 5 h study period (Figure 2A, Table S3, and Figures S49−S50) while no new adduct was observed for **AuDCC2** complexes. This result suggests that **AuDCC2** is more stable toward biological reductants than **AuDCN2**. This stability may be rationalized with respect to the presence of two strong sigma donating carbon atoms bonded to gold in **AuDCC** complexes compared with **AuDCN** complexes with one Au−C and Au−N bond.

Further evidence of stability was obtained from the electrochemical characterization of representative complexes in DMSO using Ag/AgCl reference electrodes. The cyclic voltammogram of **AuDCN2** shows a redox potential of −0.92 V, which corresponds to a reduction peak while **AuDCC2**

undergoes a pseudoreversible reduction at −1.01 V and a corresponding oxidation at −0.8 V as shown in Figure 2B. This result suggests that cyclometalation remains an important strategy to enhance the electrochemical stability of Au(III) complexes. Further, while **AuDCN2** undergoes irreversible reductions, the more sigma donor stabilized **AuDCC2** complex demonstrates redox reversibility arising from the gold(III) center and dithiocarbamate ligand interaction. Overall, the stability of complexes with [C^C-Au(III)-S^S] scaffold is demonstrated and may be useful to study protein-Au(III) complex interactions.

In Vitro Cytotoxicity. To investigate the impact of different cyclometalated scaffolds and chain lengths on cellular response, we first sought to determine the cytotoxicity of Au(III) dithiocarbamate complexes in three (3) different cancer cell lines using MTT assay. MTT (3-(4,5-dimethylth-iazol-2-yl)-2,5-diphenyl-2H-tetrazolium bromide) is a cationic lipophilic tetrazolium dye that can be reduced to formazan by metabolically active cells. In this work, aggressive cancer cell types (MDA-MB-231 triple negative breast cancer cell, BT-333 human glioblastoma, and UWB1.289 ovarian cancer cells) with limited treatment options in the clinic were treated with the eight Au(III) dithiocarbamate complexes at different concentrations within a 72-h period (Table 1, Figures S51−58). Our

Table 1. Table Showing IC$_{50}$ Values (μM) for Au(III) Dithiocarbamate Complexes in MDA-MB-231, BT-333 and UWB1.289 Cancer Cell Lines[a]

Complexes	BT-333	MDA-MB-231	UWB1.289
AuDCN1	0.013 ± 0.02	0.35 ± 0.04	2.69 ± 0.04
AuDCC1	1.99 ± 0.07	4.07 ± 0.09	>100
AuDCN2	0.68 ± 0.01	1.38 ± 0.06	2.19 ± 0.02
AuDCC2	>100	>100	31.6 ± 0.05
AuDCN6	1.38 ± 0.03	1.23 ± 0.05	2.81 ± 0.03
AuDCC6	53.70 ± 0.03	81.28 ± 0.08	>100
AuDCN12	17.78 ± 0.03	23.44+ 0.13	22.9 ± 0.05
AuDCC12	89.12 ± 0.03	>100	>100

[a]Cells were treated with freshly prepared stock solution of compound in DMSO (< 1%) Data is represented as mean ± SD (n = 6).

screening showed that there was a correlation between the carbon chain length, solubility in biological media, and anticancer activity of these complexes. Increasing the number of carbon chain length on the dithiocarbamate ligand leads to reduced solubility and cytotoxicity. Also, the cytotoxicity of **AuDCN** complexes were lower (IC$_{50}$ = 13 nM−23 μM) in all the cell lines screened compared to their corresponding **AuDCC** complexes (IC$_{50}$ = 1.99 to >100 μM). The lower IC$_{50}$ values observed for **AuDCN** complexes can be attributed to the cationic character of **AuDCN** complexes due to the significant affinity for the inner mitochondrial membrane, which has a negative redox potential.

Lipophilicity. Extending the carbon chain length of a drug can influence their physicochemical properties, and increase hydrophobic interactions, thereby impacting drug activity. To rationalize the impact of cyclometalation and alkyl chain lengths on cellular response, we computed their lipophilicity using SWISSADME software and experimentally determined the partition coefficient in an octanol−water mixture. Theoretically, the LogP values of these complexes increase with alkyl chain length for both **AuDCN** and **AuDCC** class of complexes (Figure 3A, Figure S59−S74). Regarding degree of

cyclometalation, **AuDCC** complexes with cyclometalated biphenyl framework showed lower lipophilicity compared to their cyclometalated phenylpyridine counterpart (**AuDCN**) with a similar alkyl chain. Experimentally, the partition coefficient of the complexes in a presaturated octanol−water solution was determined by measuring their affinity to each phase. The log absorbance of the HPLC trace of each phase was measured and calculated as $\log P = \frac{[\text{octanol layer}]}{[\text{water layer}]}$. The LogP values of **AuDCN1,2** and **6** were determined to be 0.19, 0.28, and 1.19 respectively while the LogP for the remaining complexes could not be determined due to greater hydrophobicity (Figure 3A). The large differences in the LogP values for both theoretical and experimental data can be due to the relativistic effect of gold that may not be accounted for in theoretical calculations due to lack of accurate parametrization models.

Cellular Uptake and Mitochondria Bioenergetics. Therapeutic efficacy of a drug-like molecule can be determined by their ability to permeate the plasma membrane and accumulate within the cells where they engage their target. Intracellular accumulation of bioactive compounds often correlates well with efficacy. Therefore, we studied the uptake of gold complexes in cells and in mitochondrial fractions. For whole cell uptake, MDA-MB-231 cells were treated with 10 μM complexes and incubated for 18 h. Gold uptake was determined by inductively coupled plasma mass spectrometry (ICP-MS). All eight complexes significantly accumulate in cells at above 5 nmol per one million cells. Cationic complexes bearing phenylpyridine backbone showed significant increase in cellular uptake compared to their neutral biphenyl counterpart with similar alkyl groups except for **AuDCN12** which showed lower cellular uptake compared to **AuDCC12** (Figure 3B). Given that gold complexes are known to alter distinct mitochondria functions, we sought to understand the effect of cyclometalation and alkyl chains on mitochondria accumulation. MDA-MB-231 cells were treated with **AuDCN2** and **AuDCC2** at 10 μM for 18 h, and we observed accumulation of gold in the mitochondria. Cationic **AuDCN2** showed a statistically significant mitochondria accumulation (11 nmol/20 million cells), compared to **AuDCC2** complexes (9 nmol/20million cells) (Figure 3C). This significant increase in mitochondria accumulation corroborate the fact that cationic species can readily accumulate intracellularly and in the mitochondria compared to neutral complexes.

Earlier reports by Mertens et al., showed that the mechanism of cytotoxic cell death of Au(III) dithiocarbamate complexes is by inhibiting mitochondrial respiration in triple negative breast cancer cells.[48] We therefore examined the effect of the gold complexes on mitochondria respiration in triple negative breast cancer cell MDA-MB-231 and ovarian cancer cell UWB1-289 by Seahorse 96XF. To determine how the degree of cyclometalation affects the OCR, **AuDCN2** and **AuDCC2** were chosen and injected pneumatically into MDA-MB-231 cancer cells. This was followed by application of oligomycin (a complex V inhibitor of the electron transport chain) to measure the minimal rate of metabolism required to support basic cell function (basal respiration); FCCP, a potent uncoupler that inhibit ATP synthesis by uncoupling the proton gradient generated by mitochondria inner membrane enabling the measurement of maximal respiration; and antimycin A/rotenone (a complex I/III inhibitor) was added
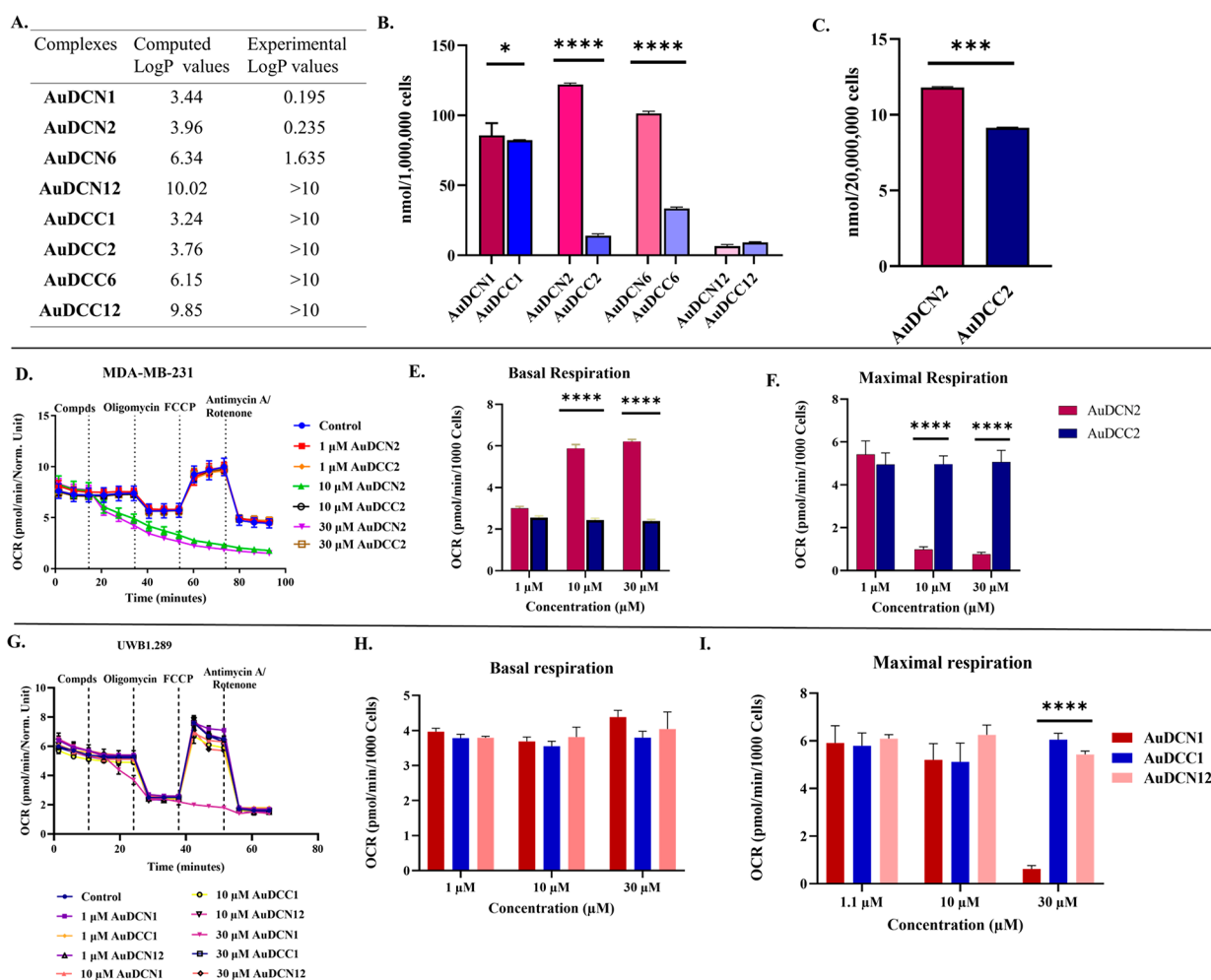
Figure 3. Impact of the degree of cyclometalation and alkyl chain-length elongation of Au(III) dithiocarbamate complexes on cellular responses. (A) Lipophilicity of Au(III) dithiocarbamate complexes determined theoretically using ADMESWISS software from Swiss Institute for Bioinformatics. LogP values shown is the consensus LogP from an average of five predictions and those performed experimentally. (B) Whole cellular uptake of Au(III) dithiocarbamate complexes in MDA-MB-231 cancer cells. Cells treated at a concentration of 10 μM for 18 h and analyzed by ICP-MS. Data plotted as mean $\pm$ s.e.m. ($n = 2$). (C) Mitochondria uptake of **AuDCN2** and **AuDCC2** in MDA-MB-231 cancer cells. Cells treated at a concentration of 10 μM for 18 h and analyzed by ICP-MS. Data plotted as mean $\pm$ s.e.m ($n = 2$). (D) Bioenergetic study of MDA-MB-231 cells after pneumatic *in vitro* treatment with **AuDCN2** and **AuDCC2**. (E–F) Key bioenergetic parameters extrapolated from Seahorse XF96 analyzer. Data plotted as mean $\pm$ s.e.m from a minimum of 12 wells. (G) Bioenergetic study of UWB1.289 cells after pneumatic *in vitro* treatment with **AuDCN1**, **AuDCN12**, and **AuDCC1**. Data plotted as mean $\pm$ standard error of the mean from a minimum of 12 wells. Unpaired student t test *$p < 0.05$, **$p < 0.01$, ***$p < 0.001$, ****$p < 0.0001$. (H–I) Key bioenergetic parameters extrapolated from Seahorse XF96 analyzer. Ordinary one-way ANOVA *$p < 0.05$, **$p < 0.1$, ***$p < 0.001$, ****$p < 0.0001$

to shut down the ETC. Analyses of the mitostress assay (Figure 3C−F) showed that **AuDCN2** rapidly inhibited oxygen consumption rate in a dose dependent manner at 10 μM compared to the control as observed from the maximal respiration (Figure 3F), whereas **AuDCC2** did not alter the rate of oxygen consumption even at 30 μM. This effect was recapitulated in ovarian cancer cell UWB1-289 where **AuDCN1**, **AuDCC1** and **AuDCN12** were studied. (Figure 3G−I) This result suggests that cationic [C^N-Au(III)-S^S]$^+$ complexes result in inhibition of OCR in cancer cells as a mode of cell cytotoxicity and increasing the alkyl chain length does not have significant effect on the oxygen consumption rate due to poor solubility of the hydrophobic gold complexes that led to reduced intracellular accumulation. We posit that strategies to improve compound solubility will enhance the potency of long alkyl chain gold(III) complexes.

Encapsulation of Au(III) Dithiocarbamate Complexes Improves Its Cytotoxicity and Cellular Uptake. In our quest to address the solubility issues of the hydrophobic Au(III) dithiocarbamate complexes, we hypothesized that nanoparticle encapsulation using biodegradable protein albumin will improve physicochemical properties and efficacy. Encapsulation with albumin has been shown to improve the pharmacodynamic properties of drug-like molecules, for example, albumin has been used to deliver cytotoxic hydrophobic Taxol, hence we prepared bovine serum albumin (BSA) encapsulated Au(III) dithiocarbamate using a desolvation method (Figure 4). The nanoparticles formed were characterized by dynamic light scattering (DLS) and scanning electron microscopy (SEM) and the cytotoxicity and cellular uptake in cancer cells measured. Briefly, BSA was dissolved in DI water, and the solution was stirred at room temperature for 15 min; desolvation was then achieved by dropwise addition of
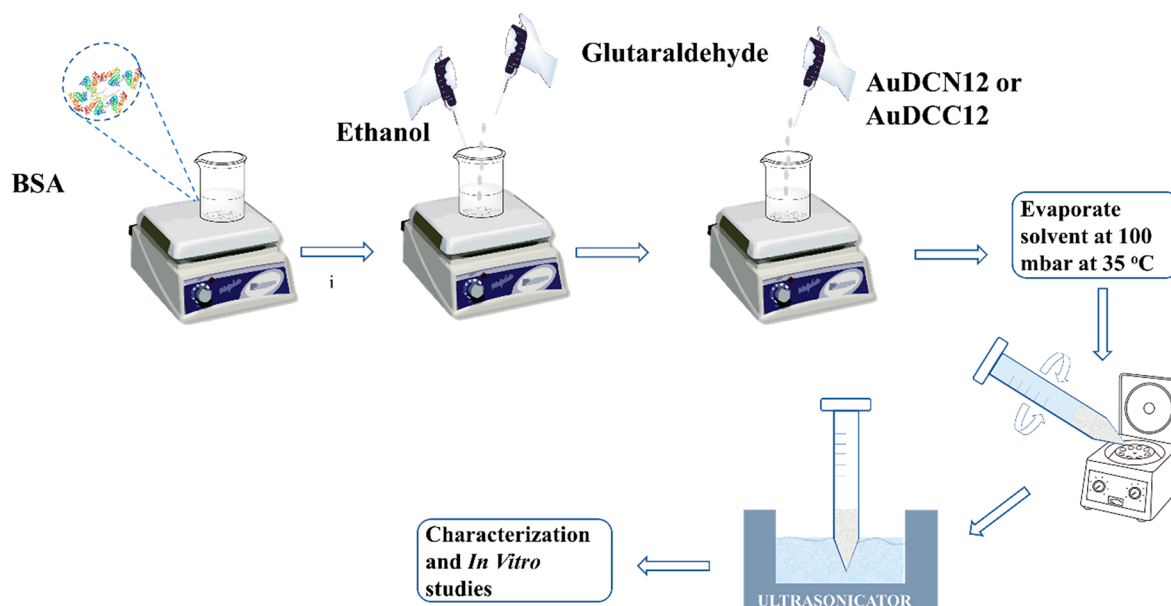
Figure 4. Flowchart showing the steps involved in bovine serum albumin encapsulation of **AuDCN12** and **AuDCC12**.

ethanol into the solution with continuous stirring at room temperature to give a cloudy suspension. This process alters the tertiary structure of albumin, leading to a decreased water solubility of albumin and enhanced phase separation.[57] Glutaraldehyde was then added to stabilize the BSA nanoparticle formed. To the suspension was then added **AuDCN12** or **AuDCC12** and the mixture was allowed to stir for 2 h. The mixture was then concentrated by gentle heating on a rotary evaporator under vacuum, transferred to an ultracentrifuge tube (MWCO 50 kDa) and centrifuged at 6000 rpm for 20 min with three successive DI water wash steps. The size, charge, and morphology of gold-loaded BSA nanoparticles were confirmed by DLS, zeta potential, and SEM analyses. As shown in Figure 5A-D, **AuDCN12/BSA** has a diameter of 225.3 ± 25.1 nm with zeta potential of 0.431 ± 0.167 mV, and **AuDCC12/BSA** has a diameter of 200.9 ± 22.1 nm with a zeta potential of 0.359 ± 0.375. SEM images were further employed to characterize gold-loaded BSA nanoparticles, and they showed the spherical morphology of the nanoconstruct formed (Figure 5I−J). This result demonstrates that BSA successfully encapsulates the gold(III) dithiocarbamate complexes. To elucidate the encapsulation efficiency and cargo loading capacity of the gold-loaded BSA nanoparticles, we prepared **AuDCN12/BSA** and **AuDCC12/BSA** at two concentrations with the loaded gold agent, **AuDCN12** or **AuDCC12** at 10 or 500 μM respectively and a concentration of 0.7 mM BSA prepared in DI water. We found that 10 μM feeding of the bioactive gold cargo resulted in approximately 2-fold higher encapsulation efficiency than that of 500 μM feeding for both nanoparticles (Table S4−S5). Of note, for **AuDCN12/BSA**, the loading capacity at 10 or 500 μM feeding was 4.03% or 28.8%, respectively (Table S4) and for **AuDCC12/BSA**, the loading capacity at 10 or 500 μM feeding was 1.96% or 14.8%, respectively (Table S5). To assess the physiological stability of the gold-loaded BSA nanoparticles, we dispersed the NPs in biologically relevant media (PBS and DMEM) and observed the solution via dynamic light scattering experiments over a period of 96 h at 37 °C. There was no precipitation observed in the solution over 96 h with little or no changes in the particle size of **AuDCN12/BSA** or **AuDCC12/BSA** as

measured by DLS (Figure 5E and 5F), pointing to optimal physiological stability and allows for use in biological models systems. The kinetic release profiles of **AuDCN12/BSA** or **AuDCC12/BSA** under slightly acidic conditions (pH 4) showed ~10−20% release of the gold cargo from the BSA nanoparticles within 48 h (Figure 5G and 5H). At pH 7.4, there was no gold cargo release under similar kinetic conditions.

With the nanoparticles in hand, we assessed the physicochemical characteristics and the attendant cellular responses that they evoke. Beyond the observation of a turbid, cloudy solution of the free **AuDCN12** or **AuDCC12** compounds in DMEM and the clear solution observed for gold-loaded BSA nanoparticles in DMEM (Figure 6A), we subjected these solutions to experimental verification by UV−vis spectroscopy ($\lambda_{max} = 254$ nm) at room temperature. The concentrations required to reach an absorbance of 1 for the gold-loaded BSA nanoparticles were significantly higher than free gold(III)-dithiocarbamate constructs (Figures S77−80). This emphasizes the enhanced solubility imparted by BSA encapsulation. Further studies to examine the impact of albumin encapsulation of **AuDCN12** or **AuDCC12** on cytotoxicity by MTT assay in MDA-MB-231 and BT-333 cancer cells was conducted. First, we determined the gold concentration in the nanoparticle construct by AAS before treatment of cancer cells. We found that the nanoparticle constructs displayed improved cytotoxicity in MDA-MB-231 and BT-333 cancer cell lines with 25−40 times reduction in IC$_{50}$ compared to free **AuDCN12** or **AuDCC12** (Figure 6B−E, Table S6). This impressive result necessitated the examination of cellular uptake in MDA-MB-231 cells. We observed a significant increase in the amount of gold content accumulation when MDA-MB-231 cells were treated with 10 μM **AuDCN12/BSA** and **AuDCC12/BSA** for 18 h (Figure 6F). This result suggests that encapsulation of drug molecules is an efficient way of improving their delivery into target cells.
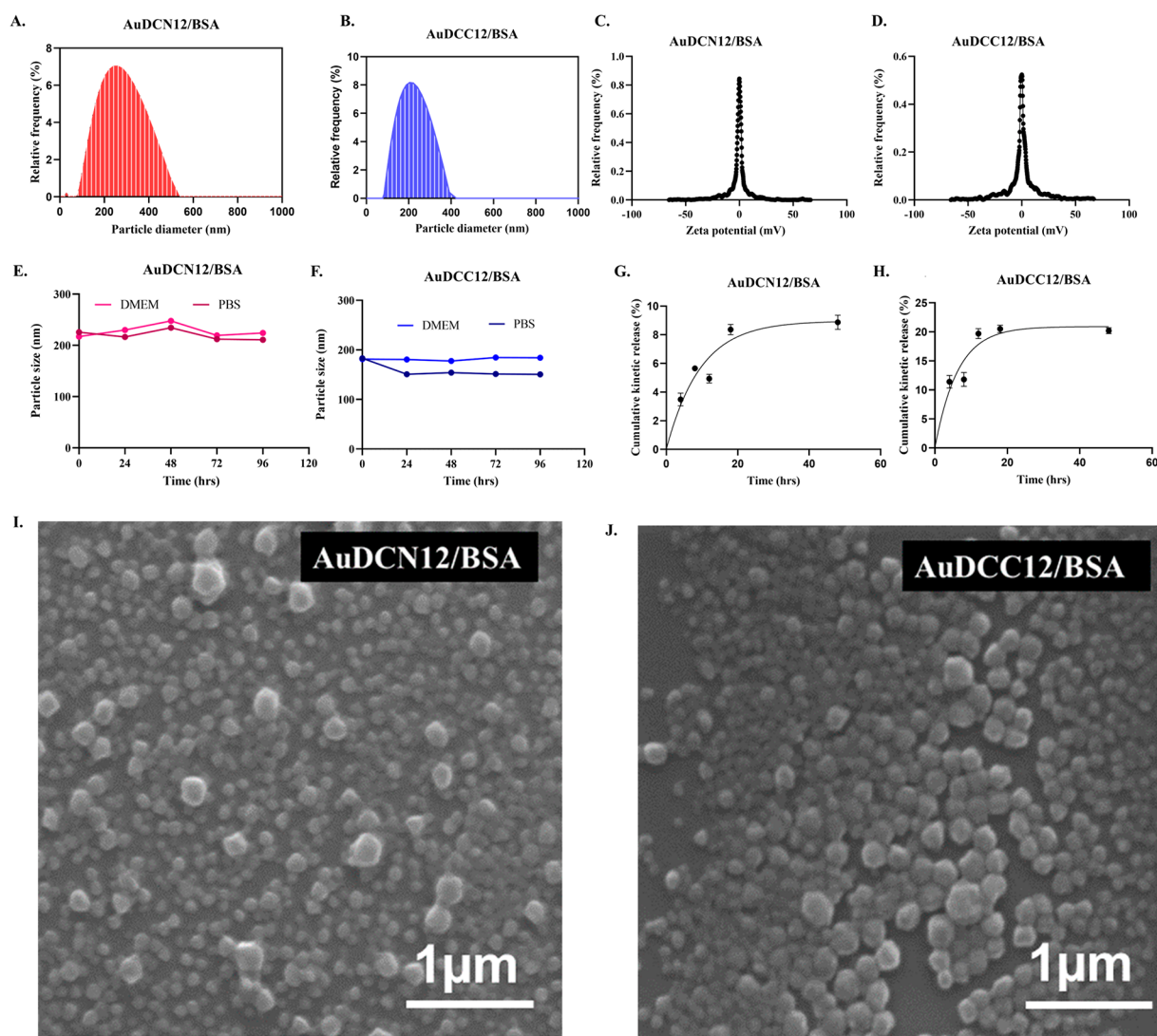
Figure 5. Physicochemical characterization of **AuDCN12/BSA** and **AuDCC12/BSA**. (A−B) Size distribution of AuDCN**12/BSA** and **AuDCC12/BSA** by DLS. (C−D) Zeta potentials of **AuDCN12/BSA** and **AuDCC12/BSA**. (E−F) Plot showing in vitro stability studies in PBS and DMEM. The particle size was measured by DLS over a period of 96 h at 37 °C. (G−H) Plot showing kinetic release profile of nanoparticle construct in PBS pH 4.0 for 48 h. Data plotted as mean ± s.e.m ($n = 2$). (I−J) SEM images of **AuDCN12** and **AuDCC12**.

CONCLUSION

In conclusion, we have studied the physicochemical impact of gold-based agents via the rational design and synthesis of gold(III) dithiocarbamate complexes with varying degrees of cyclometalation and alkyl chain lengths. We showed by cyclic voltammetry and LCMS studies that stability of Au(III) complexes can be improved through cyclometalation and that the degree of cyclometalation influences stability of Au(III) dithiocarbamate complexes with neutral complexes of the type [C^C-Au(III)-S^S] showing more solution stability than cationic [C^N-Au(III)-S^S]$^+$ complexes in a L-GSH model reaction.

Furthermore, in vitro cytotoxicity studies showed that the anticancer activity of these complexes is dependent on the degree of cyclometalation and alkyl chain length, with cationic AuDCN complexes having lower IC$_{50}$ values compared to neutral AuDCC complexes. Also, increasing alkyl chain length from methyl to dodecyl alkyl groups results in a corresponding increase in IC$_{50}$ values. This result can be explained from the affinity of cationic gold(III) dithiocarbamate complexes to the

more negative redox potential of the mitochondria and the increased lipophilicity, reduced solubility, and cellular uptake of higher alkyl chain dithiocarbamate in biological media and cancer cells. To improve these cellular responses, higher chain Au(III) dithiocarbamate complexes were encapsulated into bovine serum albumin using the desolvation method and they were characterized by DLS and SEM. The BSA encapsulation approach greatly improves the solubility in biological media, cellular uptake, and potency in MDA-MB-231 and BT-333 cancer cell lines. We believe that this approach can help in reducing the systemic toxicity, off-target effects, and enable the effective delivery of next generation gold-based chemotherapeutics to the clinic.

MATERIALS AND METHOD

Materials. All of the solvents used in the work were purchased from Greenfield Global (ACS grade). The starting Au(III) cyclometalated complex dichloro(2-phenylpyridine)gold(III) was prepared as previously reported.[58] HAuCl$_4$.3H$_2$O was purchased from ACROS Organic and stored under a nitrogen atmosphere. Sodium hexafluorophosphate and 2,2-dibromobiphenyl were purchased from
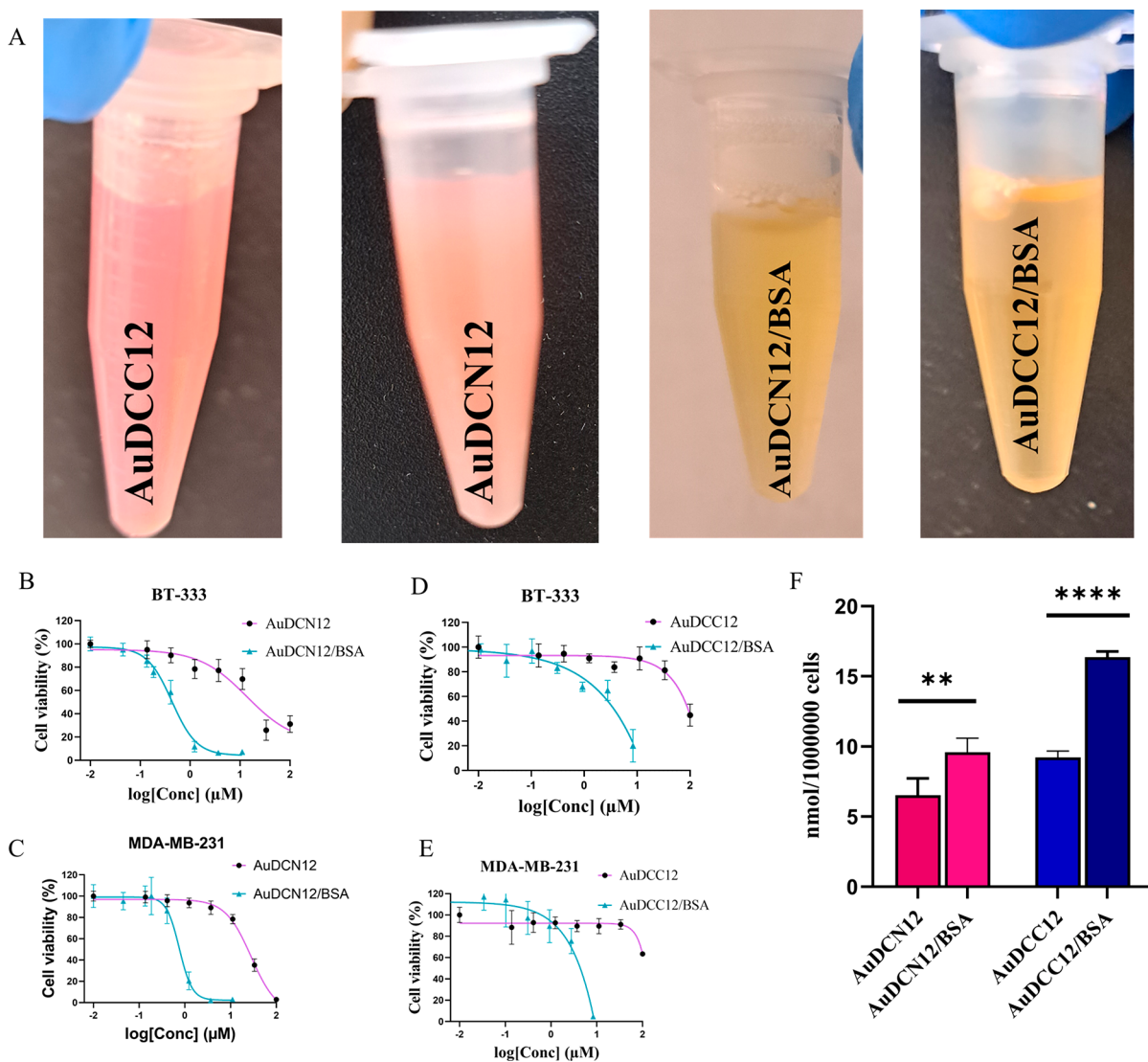
Figure 6. In vitro cytotoxicity and cellular uptake of **AuDCN/BSA** and **AuDCC12/BSA**. (A) Images showing improved solubility of encapsulated Au(III) dithiocarbamate compared to naked Au(III) dithiocarbamate. (B−E) Dose response curve showing improved cytotoxicity of BSA encapsulated Au(III) dithiocarbamate. Data plotted as mean $\pm$ SD (n = 6) F) Whole cell uptake studies. Data plotted as mean $\pm$ s.e.m (n = 2). Unpaired student t test *$p < 0.05$, **$p < 0.01$, ***$p < 0.001$, ****$p < 0.0001$.

Matrix scientific. Di-n-butyl tin dichloride, carbon disulfide, sodium dimethyl dithiocarbamate and sodium diethyl dithiocarbamate salts, dihexylamine, and didodecyl amine were purchased from Alfa Aesar. n-Butyllithium solution (1.6 M in hexane) and anhydrous ether were purchased from Sigma-Aldrich. Sodium hydroxide pellets were purchased from VWR. 3-(4,5-dimethylthiazol-2-yl)-2,5-diphenyltetrazolium bromide (MTT) was purchased from Cayman Chemicals. Bovine serum albumin, glutaraldehyde, nitric acid (trace metal grade) and hydrochloric acid (trace metal grade) were purchased from Thermo Fisher scientific. All biological supplements for media, PBS and trypsin-EDTA were purchased from Corning Inc. and used as purchased. Deuterated solvents were purchased from Cambridge Isotope Laboratories (Andover, MA). ^{1}H, ^{13}C (^{1}H-decoupled), and ^{31}P (^{1}H-decoupled) NMR spectra were recorded on a 500 MHz JEOL ECZr and Bruker Avance NEO 400 MHz spectrometer and samples calibrated for: ^{1}H NMR (CDCl$_3$ δ = 7.26 ppm), ^{13}C NMR (CDCl$_3$ δ = 77.16), and ^{31}P NMR externally referenced to H$_3$PO$_4$ δ = 0.00). Liquid chromatography mass spectra were obtained by direct flow injection (injection volume = 10 μL) using ElectroSpray Ionization (ESI) on an Advion Expression CMS MassExpress 6.7.15.1 mass spectrometer instrument in the positive mode coupled with RP-HPLC using an Agilent Technologies 1100 series HPLC

instrument and an Agilent Phase Eclipse Plus C18 column (4.6 × 100 mm; 3.5 μm particle size). All compounds were found to be ≥97% pure. Gold content was determined using Agilent 8800 QqQ Inductively coupled plasma mass spectrometry and a Varian Spectra AA100Z Atomic Absorption Spectrometer. The ICPMS has the following conditions: Tune mode = He MS/MS; Tune elements ^{7}Li, ^{89}Y, ^{95}Mo, ^{197}Au (all at 1 ppb); RF power = 1550 W, RF matching 1.8 V, sample depth 10.0 mm, Nebulizer gas 1.04 l/min, He Flow rate = 4.0 mL/min, H$_2$ Flow rate = 0.0 mL/min, OctP Bias = −20 V, OctP RF = 200 V, Energy discrimination = 5.0 V

Synthesis and Characterization. *Synthesis of Dichloro(2-phenylpyridine)gold(III).* The synthesis of dichloro(2-phenylpyridine)gold(III) was carried out using an already established protocol from our lab. Briefly, 2-phenylpyridine (76 mg, 0.492 mmol) was added to a 30 mL pressure tube containing HAuCl$_4$·3H$_2$O (0.194 g, 0.492 mmol) in water (10 mL) and the reaction was heated to 130 °C with continuous stirring for 24 h days. The precipitate formed was filtered and washed with DI H$_2$O, ethanol, and ether to give an off-white solid that was used without further purification. Yield: 0.161 g, (77.4%). ^{1}H NMR (400 MHz, DMSO-d_6) δ: 9.53 (d, J = 6, Hz, 1H), 8.44−8.38 (m, 2H), 7.98 (dd, J = 7.7, 1.7 Hz, 1H), 7.82 (dd, J = 8.1, 1.1 Hz, 1H), 7.78 (td, J = 6.3, 2.6 Hz, 1H), 7.49 (td, J = 7.5, 1.1 Hz,

1H), 7.39 (td, J = 8, 2.6 Hz, 1H). ^{13}C NMR (101 MHz, DMSO) δ: 164.41, 152.78, 148.51, 144.46, 143.47, 132.15, 130.49, 129.84, 127.24, 125.82, 122.67.

Synthesis of 9,9-Dibutyl-9-stannafluorene. A Schlenk flask (250 mL) was charged with a solution of 2,2′-dibromobiphenyl (2 g, 6.410 mmol) in 60 mL of anhydrous diethyl ether under N_2 gas at −78 °C. *n*-BuLi (1.6 M in hexane solution) (8 mL, 12.82 mmol) was added dropwise, and the temperature warmed to room temperature. The solution was stirred for 2 h after which a solution of Bu_2SnCl_2 (2.08 g, 6.859 mmol) in 2 mL of diethyl ether was added, the light-yellow solution turned white after addition, and stirring was continued overnight. Water (50 mL) was added, and the organic layer extracted, dried with $MgSO_4$, filtered, and concentrated to give a pale-yellow solid which was purified by column chromatography (100% Hexane) to give white solid. Yield: 1.29 g, 52.8%. ^{1}H NMR (500 MHz, CDCl$_3$): δ 7.96 (d, J = 10.0 Hz, 2H), 7.59 (d, 2H, J = 5 Hz, J_{H-Sn} = 40 Hz), 7.35 (dd, J = 10 Hz, 5 Hz, 2H), 7.24 (dd, J = 10, 5 Hz, 2H), 1.65 (m, 4H), 1.39 (m, 8H), 0.84 (t, J = 10 Hz, 6H). ^{13}C NMR (125 MHz, CDCl$_3$): δ 148.8, 141.2, 136.6 (J_{C-Sn} = 45 Hz), 128.9, 127.3 (J_{C-Sn} = 30.0 Hz), 122.75 (J_{C-Sn} = 34.3 Hz), 29.1, 27.3 (J_{C-Sn} = 54.9 Hz), 13.7, 12.1 (J_{C-Sn} = 360.7 Hz).

Synthesis of μ-Chlorobiphenyl Au(III). In a 50 mL round-bottomed flask fitted with a magnetic stir bar, HAuCl$_4$.3H$_2$O (200 mg, 0.519 mmol) in 10 mL of acetonitrile was added. To this yellow solution 9,9-dibutyl-9-stannafluorene (204.51 mg, 0.519 mmol) was introduced. The solution was then placed in an oil bath and stirred at reflux for 24 h. After 24 h, the precipitate formed was filtered, washed with acetonitrile (20 mL), and chloroform (20 mL) and dried to give an off-white solid. Yield for complete compound: 74.5 mg, 37.3%. ^{1}H NMR (400 MHz, DMSO-d_6) δ: 6.90 (t, J = 8 Hz, 2H), 6.99 (t, J = 4 Hz, 2 H), 7.14−7.21 (m, 4H), 7.41−7.44 (m, 6H), 7.81 (d, 8 Hz, 2H). ^{13}CNMR (101 MHz DMSO-d_6) δ: 122.07, 122.44, 127.12, 127.24, 128.67, 128.97, 133.67, 147.98, 150.89, 152.06, 156.64.

General Procedure A: Synthesis of Sodium Dialkyldithiocarbamate. Sodium dihexyldithiocarbamate and sodium didodecyl dithiocarbamate salts were prepared according to a modified procedure in the literature.[48] In a round-bottom flask, dialkylamine (1.35 mmol, 1 equiv) and NaOH (1.35 mmol, 1 equiv) were mixed with ethanol (20 mL). The mixture was sonicated to dissolve NaOH completely and placed in an ice bath at 0 °C. Carbon disulfide (2.70 mmol 2 equiv) was added dropwise, and the reaction mixture was stirred at room temperature overnight. The reaction mixture was concentrated in vacuo and used for the next step without further purification.

Dihexyldithiocarbamate. Yield: quantitative. ^{1}H NMR (400 MHz, CDCl$_3$) δ: 3.92 (t, 4H, J = 8 Hz), 1.72−1.65 (m, 4H), 1.36−1.25 (m, 12H), 0.88 (t, J = 8 Hz, 6H). ^{13}C NMR (101 MHz, CDCl$_3$) δ: 208.08, 54.75, 31.68, 26.99, 26.79, 22.69, 14.06.

Didodecyldithiocarbamate. Yield: quantitative. ^{1}H NMR (400 MHz, Chloroform-d) δ: 3.91 (t, 4H J = 8 Hz), 1.65−1.74 (m, 4H), 1.23−1.31 (m, 36H), 0.88 (t, J = 8 Hz, 6H). ^{13}C NMR (101 MHz, CDCl$_3$) δ: 207.87, 58.39, 54.83, 31.98, 29.88, 29.79, 29.57, 29.45, 27.24, 27.03, 22.73, 18.39, 14.14.

General Procedure B: Synthesis of AuDCN Complexes. Dichloro(2-phenylpyridine)gold(III) (40 mg, 0.094 mmol) was suspended in 20 mL of MeOH in a 250 mL Erlenmeyer flask and stirred at room temperature. A separate solution of the corresponding sodium dithiocarbamate salt (0.094 mmol) was dissolved in 10 mL of MeOH and added dropwise. The mixture gradually turned yellow upon the addition of the dithiocarbamate solution. The reaction mixture was stirred at room temperature overnight. A saturated solution of NaPF$_6$ in DI H$_2$O was made and added to the MeOH mixture. Excess distilled water was added, until a precipitate was observed. The solution was filtered, and the solid was washed with distilled water and diethyl ether and dried to afford the corresponding AuDCN complexes.

General Procedure C: Synthesis of AuDCC Complexes. In a 50 mL round-bottomed flask equipped with a magnetic stirrer, biphenyl[AuC)Cl]$_2$ (40 mg, 0.052 mmol) and THF (9 mL) were added. The reaction mixture was cooled to 0 °C in an ice bath and

sodium dialkyldithiocarbamate (0.104 mmol, 2 equiv) was added. The reaction was stirred for 20 min and monitored by TLC (100% DCM) for completion. After completion of reaction, the solution was filtered through Celite and concentrated to yield the product. **AuDCC6** and **AuDCC12** were purified on silica gel combiflash 0−25% DCM/Hexane.
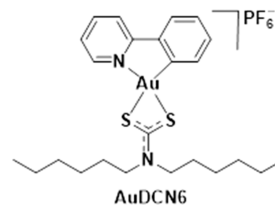
AuDCN1.

AuDCN1

Prepared as described in the general procedure B. Yield: 50.5 mg, 86.6%. ^{1}H NMR (500 MHz, Acetonitrile-d_3) δ: 8.60 (d, J = 5 Hz 1H), 8.31 (t, J = 10 Hz 1H), 8.23 (d, J = 5 Hz 1H), 7.91 (d, J = 5 Hz, 1H), 7.60 (t, J = 10 Hz 1H), 7.52 (t, J = 10, 1H), 7.39 (t, J = 10 Hz, 1H), 7.18 (d, J = 5, Hz, 1H), 3.46, (s, 3H), 3.45 (s, 3H). ^{13}C NMR (101 MHz, DMSO-d_6) δ: 192.77, 163.12, 150.97, 149.61, 143.86, 143.66, 132.13, 129.06, 128.00, 127.11, 126.05, 122.26, 41.92, 40.02. ^{31}P NMR (162 MHz, CD$_3$CN) δ: −144.62. ^{19}F NMR (376 MHz, CD$_3$CN) δ −72.05. Purity was determined to be >97% by RP-HPLC: R_f = 6.9 min using the following method: Flow rate: 1 mL/min; λ = 260 nm; Eluent A = DI water with 0.1% trifluoroacetic acid; Eluent B = Acetonitrile with 0.05% formic acid; Solvent Gradient: 0−16 min (0:100 H$_2$O: can). Sixteen min until the end of run (100:0 H$_2$canACN). ESI+ MS (found) = 471.1 [M − PF$_6$]$^+$ (calcd = 471.03).

AuDCN2.

AuDCN2
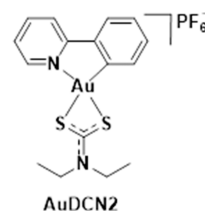
Prepared as described in the general procedure B. Yield: 45 mg, 73.7%. ^{1}H NMR (500 MHz, Acetonitrile-d_3) δ: 8.61 (d, J = 5 Hz, 1H), 8.34 (t, J = 10 Hz, 1H), 8.22 (d, J = 5 Hz, 1H), 7.93 (d, J = 5 Hz, 1H), 7.60 (t, J = 10 Hz, 1H), 7.53 (t, J = 10 Hz, 1H), 7.44 (t, J = 10 Hz, 1H), 7.20 (d, J = 5 Hz, 1H), 3.86 (q, J = 10, 5 Hz, 2H), 3.87(q, J = 10, 5 Hz) 1.44−1.36 (m, 6H). ^{13}C NMR (101 MHz, CD$_3$CN) δ: 194.23, 164.54, 152.02, 149.78, 144.59, 144.34, 133.05, 129.95, 128.84, 127.55, 126.47, 122.89, 49.29, 47.74, 12.31, 12.02. ^{31}P NMR (162 MHz, CD$_3$CN) δ: −144.67. ^{19}F NMR (376 MHz, CD$_3$CN) δ: −72.06, −73.93. Purity was determined to be >97% by RP-HPLC: R_f = 7.86 min using the following method: Flow rate: 1 mL/min; λ = 260 nm; Eluent A = DI water with 0.1% trifluoroacetic acid; Eluent B = Acetonitrile with 0.05% formic acid; Solvent Gradient: 0−16 min (0:100 H$_2$O: ACN). Sixteen min until end of run (100:0 H$_2$O: ACN). ESI+ MS (found) = 499.2 [M − PF$_6$]$^+$ (calcd = 499.04).

AuDCN6.

AuDCN6

Prepared as described in the general procedure B. Yield: 81.7%. ^{1}H NMR (500 MHz, Acetonitrile-d_3) δ: 8.59 (d, 1H), 8.32 (t, J = 10 Hz, 1H), 8.21 (d, J = 10 Hz, 1H), 7.92 (d, J = 5, Hz, 1H), 7.60 (t, J = 10 Hz, 1H), 7.52 (t, J = 10 Hz, 1H), 7.41 (t, J = 10 Hz, 1H), 7.19 (d, J = 5 Hz, 1H), 3.85−3.75 (m, 4H), 1.87−1.78 (m, 4H), 1.45−1.32 (m, 12H), 0.94−0.91 (m, 6H). ^{13}C NMR (101 MHz, CD$_3$CN) δ: 195.00,

152.12, 149.85, 144.36, 133.05, 129.97, 128.91, 127.58, 126.47, 122.92, 117.88, 54.48, 52.83, 31.57, 27.42, 27.13, 26.54, 22.79, 13.84, 13.35. ^{31}P NMR (162 MHz, CD$_3$CN): −144.62. ^{19}F NMR (376 MHz, CD$_3$CN) δ: −72.04. Purity was determined to be >97% by RP-HPLC: R_f = 11.34 min using the following method: Flow rate: 1 mL/min; λ = 260 nm; Eluent A = DI water with 0.1% trifluoroacetic acid; Eluent B = Acetonitrile with 0.05% formic acid; Solvent Gradient: 0−16 min (0:100 H$_2$O: ACN). Sixteen min until end of run (100:0 H$_2$O: ACN). ESI+ MS (found) = 611.2 [M − PF$_6$]$^+$ (calculated = 611.18).

AuDCN12.

AuDCN12
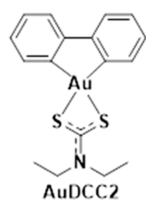
Prepared as described in the general procedure B. Yield: 36.5 mg, 42%. ^{1}H NMR (500 MHz, Chloroform-d): δ 8.39 (d, J = 5 Hz, 1H), 8.29 (t, J = 10 Hz, 1H), 8.10 (d, J = 5 Hz, 1H), 7.72 (d, J = 5 Hz, 1H), 7.64 (t, J = 10 Hz, 1H), 7.40 (t, J = 10 Hz, 1H), 7.24 (d, J = 5 Hz, 1H), 6.95 (d, J = 5 Hz, 1H), 3.78 (m, 4H), 1.87−1.79 (m, 4H), 1.32−1.20 (m, 36H), 0.87 (t, J = 5 Hz, 6H). ^{31}P NMR (162 MHz, CDCl$_3$): −143.59. ^{19}F NMR (376 MHz, CDCl$_3$): δ −70.52. Purity was determined to be >97% by RP-HPLC: R_f = 16.2 min using the following method: Flow rate: 1 mL/min; λ = 260 nm; Eluent A = DI water with 0.1% trifluoroacetic acid; Eluent B = Acetonitrile with 0.05% formic acid; Solvent Gradient: 0−20 min (0:100 H$_2$O: ACN). Twenty min until end of run (100:0 H$_2$O: ACN). ESI+ MS (found) = 799.4 [M − PF$_6$]$^+$ (calculated = 799.27).

AuDCC1.

AuDCC1
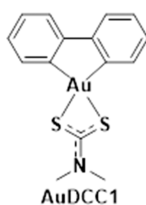
Prepared as described in the general procedure C. Yield = 45 mg, 80.5%. R_f = 0.44 in 50% Hexane: DCM. ^{1}H NMR (400 MHz, DMSO-d_6) δ: 7.56 (d, J = 8 Hz, 2H), 7.22 (t, J = 8 Hz, 2H), 7.17 (d, J = 8 Hz, 2H), 7.01 (t, J = 8 Hz, 2H), 3.44 (s, 6H). ^{13}C NMR (101 MHz, CDCl$_3$) δ: 205.13, 153.28, 153.16, 131.22, 127.41, 127.11, 121.73, 40.95. Purity was determined to be >97% by RP-HPLC: R_f = 10.87 min using the following method: Flow rate: 1 mL/min; λ = 260 nm; Eluent A = DI water with 0.1% trifluoroacetic acid; Eluent B = Acetonitrile with 0.05% formic acid; Solvent Gradient: 0−15 min (0:100 H$_2$O: ACN). 15−20 min until the end of run (100:0 H$_2$O: ACN). ESI+ MS (Found) = 470.1 (calculated) = 470.03.

AuDCC2.

AuDCC2

Prepared as described in the general procedure C. Yield: 36 mg, 70%. R_f = 0.52 in 50% Hexane: DCM. ^{1}H NMR (400 MHz, DMSO-d_6): δ 7.56 (d, J = 7.5 Hz, 2H), 7.22 (t, J = 7.5 Hz, 2H), 7.16 (d, J = 7.5 Hz, 2H), 7.01 (t, J = 7.4 Hz, 2H), 3.85 (q, J = 7.2 Hz, 4H), 1.34 (t, J = 7.1 Hz, 6H). ^{13}C NMR (101 MHz, DMSO) δ: 199.82, 153.24, 153.07, 131.29, 128.08, 127.87, 122.49, 47.16, 12.62. Prepared as described in the general procedure C. Yield ^{1}H NMR (400 MHz, DMSO-d_6) δ 7.56 (d, J = 8 Hz, 2H), 7.22 (t, J = 8 Hz, 2H), 7.17 (d, J = 8 Hz, 2H), 7.01 (t, J = 8 Hz, 2H), 3.44 (s, 6H). ^{13}C NMR (101 MHz, DMSO) δ:

153.16, 131.37, 128.13, 127.93, 122.55, 41.58. Purity was determined to be >97% by RP-HPLC: R_f = 9.5 min using the following method: Flow rate: 1 mL/min; λ = 260 nm; Eluent A = DI water with 0.1% trifluoroacetic acid; Eluent B = Acetonitrile with 0.05% formic acid; Solvent Gradient: 0−10 min (0:100 H$_2$O: ACN). Ten min until the end of the run (100:0 H$_2$O: ACN). ESI+ MS (found) = 498 [M + 1]$^+$ (calculated = 498.04).

AuDCC6.

AuDCC6
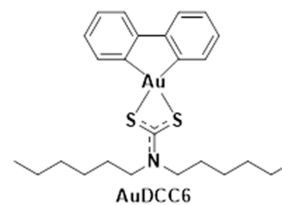
Prepared as described in the general procedure C. Yield: 40 mg, 92.8%. R_f = 0.61 in 50% Hexane: DCM. ^{1}H NMR (500 MHz, Chloroform-d) δ: 7.44 (d, J = 8 Hz, 2H), 7.28−7.25 (m, 2H), 7.18 (d, J = 16.0 Hz, 2H), 6.98 (t, J = 8 Hz, 2H), 3.69 (t, J = 8.0 Hz, 4H), 1.81−1.71 (m, 4H), 1.36 (d, J = 12.2 Hz, 12H), 0.93 (t, 8 Hz, 6H). ^{13}C NMR (126 MHz, CHLOROFORM-d) δ: 203.59, 153.62, 153.26, 131.31, 127.40, 127.16, 121.76, 52.14, 31.46, 27.23, 26.59, 22.63, 14.10. Purity was determined to be >97% by RP-HPLC: R_f = 11.43 min using the following method: Flow rate: 1 mL/min; λ = 260 nm; Eluent A = DI water with 0.1% trifluoroacetic acid; Eluent B = Acetonitrile with 0.05% formic acid; Solvent Gradient: 0−20 min (0:100 H$_2$O: ACN). Twenty min until end of run (100:0 H$_2$O: ACN). ESI+ MS (found) = 610.1 [M + 1]$^+$ (calculated = 610.65).

AuDCC12.

AuDCC12
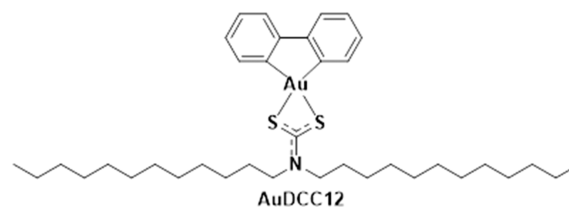
Prepared as described in the general procedure C. Yield = 55 mg, 69%. R_f = 0.65 in 50% Hexane: DCM. ^{1}H NMR (400 MHz, Chloroform-d) δ: 7.44 (d, J = 8 Hz, 2H), 7.28 (s, 1H), 7.19 (t, J = 8 Hz, 2H), 6.99 (t, J = 7.4 Hz, 2H), 3.75−3.68 (m, 3H), 1.80 (t, J = 8 Hz, 4H), 1.43−1.20 (m, 36H), 0.88 (t, J = 8 Hz, 6H). ^{13}C NMR (101 MHz, CDCl$_3$) δ: 203.53, 153.52, 153.18, 131.21, 127.32, 127.07, 121.68, 77.35, 77.04, 76.72, 52.03, 31.94, 29.65, 29.57, 29.49, 29.38, 29.23, 27.17, 26.84, 22.72, 14.16. Purity was determined to be >97% by RP-HPLC: R_f = 11.19 min using the following method: Flow rate: 1 mL/min; λ = 260 nm; Eluent A = DI water with 0.1% trifluoroacetic acid; Eluent B = methanol with 0.05% formic acid; Solvent Gradient: 0−5 min (70:30 H$_2$O: MeOH). 5−7 min (50:50 H$_2$O: MeOH), 7−10 min (0:100 H$_2$O: MeOH), 10−15 min (20:80 H$_2$O: MeOH) 15 min until the end of the run (100:0 H$_2$O: MeOH).

Physical and Chemical Characterization. *X-ray Crystallography.* Crystal for complexes **AuDCN6** and **AuDCC1** were grown at room temperature from a vapor diffusion of chloroform into diethyl ether. Crystals were mounted using polyisobutene oil on the end of a glass fiber, which had been mounted to a copper pin using an electrical solder after careful selection of suitable crystals by microscopic examination through crossed polarizers. The selected crystal was transferred to the cold gas stream of a liquid nitrogen cryostat[59,60] diffraction collected by a Bruker D8 Venture diffractometer with graded multilayer focused MoKα X-rays (λ = 0.71073 Å). Lorentz-polarization effects was corrected by integrating, scaling, merging and correcting the raw data gotten from the diffractometer using APEX3 package.[61−63] Space group determination, structure solution and refinement was determined with SHELXT and SHELXL while ellipsoid plots were drawn using SHELXTL-XP.[64−66] The positioning of hydrogen atoms was determined after calculation and refining using a riding model with their isotropic displacement parameters (U_{iso}) determined based on the atom to which they were

attached while anisotropic displacement parameters were to refine non-hydrogen atoms. The structures, deposited in the Cambridge Structural Database, were checked for missed symmetry, twinning, and overall quality with PLATON,[67] an R-tensor,[68] and finally validated using CheckCIF.[67] See Figures 1 and S1−S3 and Tables S1−S3 for structural details.

LCMS Stability Studies with L-Glutathione. L-Glutathione (1 mM in water) was mixed with **AuDCN2** or **AuDCC2** (1 mM in acetonitrile) to make a 0.5 mM equimolar solution. The solution was then subjected to LCMS analysis with readings taken every hour for 5 h using an Advion expression CMS mass express 6.7.15.1 coupled with RP-HPLC using an Agilent Technologies 1100 series HPLC instrument and an Agilent Phase Eclipse Plus C18 column (4.6 mm × 100 mm; 3.5 μm particle size). The data was analyzed using Advion data express and Graphpad 9.5.1 software.

Electrochemical Studies. Electrochemical analysis of **AuDCN2** and **AuDCC2** was carried out using a CH instruments 650E potentiostat. The electrodes used are a 3 mm glassy carbon working electrode (CHI104), a 3 mm Ag/AgCl reference electrode (CHI111), and a 3 mm platinum wire counter electrode (CHI115). **AuDCN2** and **AuDCC2** were prepared as a 5 mM solution in DMSO with 0.1 M tetrabutylammonium hexafluorophosphate (NBu$_4$PF$_6$) as the supporting electrolyte. Prior to each measurement, the samples were purged with nitrogen for 30 min to eliminate any dissolved oxygen in the solution. The electrochemical measurements were taken at a scan rate of 0.1 V/s with a three-segment sweep and a sample interval of 0.001 V. The quiet time was set to 2 s and sensitivity 1 × 10^{-5} A/V. Data were analyzed with GraphPad Prism 9.5.1

Lipophilicity. To determine the LogP for the gold(III) dithiocarbamate complexes, a stock solution (1000 μM) was prepared in acetonitrile. In a 1.5 mL Eppendorf tube was added 400 μL of presaturated octanol, 400 μL of DI water, and 200 μL of the test sample was added. The sample was agitated for 30 min and centrifuged at 10,000 g at 23 °C for 15 min, and the octanol layer was separated from the water layer. HPLC trace of each layer was taken, and the partition coefficient of the complexes in a presaturated octanol−water solution was determined by measuring their affinity to each phase. The log absorbance of the HPLC trace of each phase was measured and calculated using $\log P = \frac{(\text{absorbance of octanol layer})}{(\text{absorbance of water layer})}$.

In Vitro Biological Assay. *Cell Culture.* MDA-MB-231 was purchased from ATCC, while BT-333 and UWB1.289 were generous gifts from Dr. Gilles Berger and Dr. Jill Kolesar, respectively. MDA-MB-231, BT-333 cancer cells were grown in DMEM supplemented with 10% FBS, 1% amphotericin B and 1% penicillin/streptomycin while UWB1.289 cancer cells were grown in Lomza's MEGM + RPMI mixture containing 3% FBS, 1% amphotericin B and 1% penicillin/streptomycin and kept in an incubator at 37 °C with 5−10% CO$_2$. All supplements along with PBS and trypsin-EDTA were purchased from Corning Inc. and used as purchased.

In Vitro Cytotoxicity. The cytotoxicity of the eight Au(III) dithiocarbamate complexes was performed in MDA-MB-231, BT-333, and UWB1.289 cancer cells. Cells were harvested after reaching 80% confluency via trypsinization. Harvested cells were then suspended in 10 mL of the appropriate medium, centrifuged at 2000 rpm for 5 min, pellet removed, and then resuspended in 5 mL of the same medium. Cell plating was carried out at a density of 4,000 cells/well in a 96-well clear bottom plate, allowed to adhere overnight at 37 °C with 5−10% CO$_2$ before addition of compounds. All the eight Au(III) dithiocarbamate complexes were prepared fresh as 1 mM stock solution in DMSO and diluted with appropriate media to the working concentration of 300 μM. The compounds were then added at seven concentrations with a 3× serial dilution starting at 100 μM for the highest concentration and incubated at 37 °C for 72 h with 5−10% CO$_2$. After 72 h, the media were removed and replaced with a solution of MTT (100 μL and incubated for 4 h at 37 °C with 5−10% CO$_2$. The dye was removed from each well and 100 μL of DMSO was added to induce cell lysis. The plates were read using a Biotek Synergy H1 Plate Reader at 570 nm (peak absorbance) and the data plotted as mean ± s.e.m (6 technical replicate) using Graphpad 9.5.1. Similarly,

the cytotoxicities of **AuDCN12/BSA** and **AuDCC12/BSA** were determined in MDA-MB-231 and UWB1.289 using the procedure described above with a starting concentration of 15 μM.

Mitochondrial Metabolism Analysis with Seahorse XF96 Analysis. For the mito-stress experiment, MDA-MB-231 and UWB1.289 cells were seeded at 30,000 cells/wells (100 μL) and allowed to adhere overnight at 37 °C with 5−10% CO$_2$. Stock solutions of **AuDCN2** and **AuDCC2** (1 mM) were prepared in DMSO and diluted to a working concentration of 100 μM with a Seahorse XF96 assay buffer. The assay was performed using a pneumatic injection of both complexes, with the final injection concentrations of 30 μM, 10 μM, and 1 μM. This was followed by injection of oligomycin (1.5 μM), FCCP (0.6 μM) and rotenone/antimycin A (0.5 μM). The metabolic parameters were calculated based on the reading gotten from a minimum of 12 wells and the data plotted as mean ± SD using Graphpad 9.5.1

Whole Cellular Uptake. MDA-MB-231 cells (1 × 10^6 cells/well) were seeded in a 6 well clear bottom plate with a final volume of 2.5 mL and allowed to adhere overnight at 37 °C. Gold(III) dithiocarbamate complexes and BSA encapsulated Au(III) dithiocarbamate were prepared as a stock in DMSO and added to each well at a final concentration of 10 μM. After 18 h of treatment cells were collected via trypsinization and centrifuged at 2000 rpm for 5 min. The pellets formed were suspended in 1 mL of DMEM, transferred to a 1.5 mL Eppendorf tube, and centrifuged a second time at 2000 rpm for 5 min. The media was decanted, and the pellets washed with PBS (1 mL × 2). The pellets were stored at −20 °C until further analysis. Prior to analysis, the pellets were suspended in 300 μL of aqua regia and digested for 4 h at 60 °C. The solution was allowed to cool to room temperature and diluted appropriately and subjected to analysis with ICP-MS. Cellular gold concentration were expressed as nmol of Au per million cells. Data is plotted as mean ± s.e.m ($n = 2$) using Graphpad Prism 9.5.1

Mitochondrial Uptake. MDA-MB-231 (20 × 10^6) were treated with 10 μM **AuDCN2** and **AuDCC2** at 37 °C. After 18 h of incubation, the media was removed and the cells were washed with PBS solution (1 mL × 3), and the cells were harvested via trypsinization. Extraction of mitochondria was carried out according to the procedures/protocol of the mitochondria extraction kit (ThermoFisher Scientific). The mitochondria pellets collected were digested with aqua regia (300 μL) for 4 h at 60 °C and then diluted to the appropriate concentration as needed. The solution was thereafter subjected to ICP-MS for analysis. Mitochondria gold concentration were expressed as nmol of Au per million cells. Data is plotted as mean ± s.e.m ($n = 2$) using Graphpad Prism 9.5.1

Encapsulation of Gold(III) Dithiocarbamate Complexes with Bovine Serum Albumin. For the BSA encapsulation of Au(III) dithiocarbamate complexes, 100 mg of bovine serum albumin (pH 7.0) was dissolved in DI water (2 mL), the solution was stirred at room temperature for 15 min, ethanol (4 mL) was added gradually with continuous stirring, and the clear solution became milky; 18 μL of 50% glutaraldehyde was then added to stabilize the BSA nanoparticle formed. **AuDCN12** or **AuDCC12** (10 μM, 500 μM, and 2 mM) dissolved in acetone were added to different batches, and the mixture was allowed to stir at room temperature for 2 h, concentrated under vacuum, and transferred to an ultracentrifuge tube (MWCO 50 kDa) The solution was centrifuged at 6000 rpm for 20 min with three successive DI water wash steps to give the respective BSA-encapsulated Au(III) dithiocarbamate.

BSA Nanoparticle Characterization. To determine the particle size of the Au(III) dithiocarbamate BSA nanoparticle formed, **AuDCN12** (33 μM) or **AuDCC12** (24 μM) was diluted in 1 mL of ultrapure water. The particle size and zeta potential were determined using Litesizer Anton−Paar particle size analyzer at 25 °C. Prior to measurement, the sample was sonicated for 1 min to avoid aggregation of nanoparticles.

Kinetic Release Profile. Using the 500 μM prepared **AuDCN12/BSA** and **AuDCC12/BSA**, 1.0 mL of test compound and 1 mL of PBS were added to a 3.5 kDa dialysis membrane (the dialysis membrane was plunged into DI water overnight before use), and the

membrane was suspended in a beaker containing 30 mL of PBS adjusted to pH 4.0 with 1 M HCl. At different time points, 0.5 mL of samples were drawn out from the beaker and replaced with equal volume of PBS. The samples taken were further digested with 70% HNO3 and concentration determined using AAS. Data plotted as mean ± s.e.m (n = 2).

Stability of AuDCN12/BSA and AuDCC12/BSA Using DLS. Using the 500 μM prepared **AuDCN12/BSA** and **AuDCC12/BSA**, 1 mL of test sample was added to 1 mL of DMEM or PBS solution and the NP size were measured every day for 5 days using DLS. Prior to measurement, the sample was sonicated for 1 min to avoid aggregation of nanoparticles.

UV−vis Solubility Studies in DMEM. Stock solutions of AuDCN12 and AuDCC12 (2.5 mM) were prepared in DMSO and serially diluted with DMEM to appropriate concentration before absorption measurement was taken with a UV−vis spectrophotometer at 37 °C. Similarly, gold-loaded BSA nanoparticles were prepared in water and diluted with DMEM to the appropriate concentration before absorbance reading. Prior to absorbance reading, the instrument was blanked with a DMEM, and measurement taken at λ_{max} 254 nm.

Scanning Electron Microscopy. AuDCN12 and **AuDCC12** were first sonicated for 5 min for proper dispersion in solution. A droplet of each sample was then micropipetted and deposited onto a silicon wafer chip (Ted Pella, Redding, CA, USA) which surface was priorly made hydrophilic by glow discharge (EM ACE600, Leica, Wetzlar, Germany). The samples were then left to dry at air before sputter coating with 5 nm of platinum (EM ACE600, Leica, Wetzlar, Germany). Imaging in the scanning electron microscope (SEM, Quanta 250 FE-SEM, FEI/ThermoFisher Scientific, Hillsboro, OR, USA) was conducted at 5 kV accelerating voltage for proper surface sensitivity.

Determination of Gold Concentration in Nanoconstructs. To a 50 μL solution of **AuDCN12/BSA** and **AuDCC12/BSA** was added 100 μL of 70% HNO_3 (trace metal grade), and the sample was digested at 60 °C for 4 h. The sample was cooled to room temperature and diluted appropriately with 1% HNO_3 before analyzing on a Varian Spectra AA100Z Atomic Absorption Spectrometer. The analysis was performed in duplicate, and the result analyzed with Graphpad 9.5.1

■ ASSOCIATED CONTENT

Ⓢ Supporting Information

The Supporting Information is available free of charge at https://pubs.acs.org/doi/10.1021/acsami.3c10025.

> Crystal data and structure refinement for compounds **AuDCN6** and **AuDCC1**; ^{1}H, ^{13}C, ^{31}P spectra, HPLC traces, dose response curves for the Au(III) dithiocarbamate complexes; standard curve for cellular and mitochondria uptake studies (PDF)

■ AUTHOR INFORMATION

Corresponding Author

Samuel G. Awuah − *Department of Chemistry, University of Kentucky, Lexington, Kentucky 40506, United States; Center for Pharmaceutical Research and Innovation and Department of Pharmaceutical Sciences, College of Pharmacy and Markey Cancer Center, University of Kentucky, Lexington, Kentucky 40536, United States;* ⓞ orcid.org/0000-0003-4947-7283; Email: awuah@uky.edu

Authors

Adedamola S. Arojojoye − *Department of Chemistry, University of Kentucky, Lexington, Kentucky 40506, United States*

Breyanna Walker − *Department of Chemistry, University of Kentucky, Lexington, Kentucky 40506, United States*

James C. Dawahare − *Department of Chemistry, University of Kentucky, Lexington, Kentucky 40506, United States*

Maame Abena O. Afrifa − *Department of Biomedical Engineering, University of Kentucky, Lexington, Kentucky 40506, United States*

Sean Parkin − *Department of Chemistry, University of Kentucky, Lexington, Kentucky 40506, United States*

Complete contact information is available at:
https://pubs.acs.org/10.1021/acsami.3c10025

Author Contributions

Conceptualization, A.S.A. and S.G.A.; methodology, A.S.A. and S.G.A.; synthesis and characterization, A.S.A, B.W, J.C.D.; X-ray crystallography, S.R.P.; Biological assays, A.S.A., B.W., J.C.D.; Nanoparticle synthesis and characteristics, A.S.A., M.A.O.A, Electrochemistry, A.S.A.; writing original draft preparation, A.S.A. and S.G.A.; writing review and editing, A.S.A. and S.G.A.; supervision, S.G.A.; funding acquisition, S.G.A.

Notes

The authors declare the following competing financial interest(s): S.G.A. has patents pending to University of Kentucky Research Foundation. S.G.A. serves on the advisory board and is Chief Science Officer for Phronesis AI.

■ ACKNOWLEDGMENTS

■ REFERENCES

(1) Steinbrueck, A.; Sedgwick, A. C.; Brewster, J. T.; Yan, K.-C.; Shang, Y.; Knoll, D. M.; Vargas-Zúñiga, G. I.; He, X.-P.; Tian, H.; Sessler, J. L. Transition Metal Chelators, Pro-Chelators, and Ionophores as Small Molecule Cancer Chemotherapeutic Agents. *Chem. Soc. Rev.* **2020**, 49, 3726−3747.

(2) Nussbaumer, S.; Bonnabry, P.; Veuthey, J.-L.; Fleury-Souverain, S. Analysis of Anticancer Drugs: A Review. *Talanta* **2011**, 85, 2265−2289.

(3) Sritharan, S.; Sivalingam, N. A Comprehensive Review on Time-Tested Anticancer Drug Doxorubicin. *Life Sci.* **2021**, *278*, 119527.

(4) Fortin, S.; Bérubé, G. Advances in the Development of Hybrid Anticancer Drugs. *Expert Opin Drug Discovery* **2013**, *8*, 1029−1047.

(5) Siegel, R. L.; Miller, K. D.; Wagle, N. S.; Jemal, A. Cancer Statistics, 2023. *CA Cancer J. Clin.* **2023**, *73*, 17−48.

(6) Loehrer, P. J.; Einhorn, L. H. Cisplatin. *Ann. Int. Med.* **1984**, *100*, 704−713.

(7) Prestayko, A. W.; D'aoust, J.; Issell, B.; Crooke, S. Cisplatin (Cis-Diamminedichloroplatinum II). *Cancer Treat. Rev.* **1979**, *6*, 17−39.

(8) Einhorn, L. H. Treatment of Testicular Cancer: A New and Improved Model. *J. Clin. Oncol.* **1990**, *8*, 1777−1781.

(9) Lippard, S. J. Chemistry and Molecular Biology of Platinum Anticancer Drugs. *Pure Appl. Chem.* **1987**, *59*, 731−742.

(10) Wheate, N. J.; Walker, S.; Craig, G. E.; Oun, R. The Status of Platinum Anticancer Drugs in the Clinic and in Clinical Trials. *Dalton Trans.* **2010**, *39*, 8113−8127.

(11) Mjos, K. D.; Orvig, C. Metallodrugs in Medicinal Inorganic Chemistry. *Chem. Rev.* **2014**, *114*, 4540−4563.

(12) Komeda, S.; Casini, A. Next-Generation Anticancer Metallodrugs. *Curr. Top. Med. Chem.* **2012**, *12*, 219−235.

(13) Muhammad, N.; Guo, Z. Metal-Based Anticancer Chemotherapeutic Agents. *Curr. Opin. Chem. Biol.* **2014**, *19*, 144−153.

(14) Wang, Y.; Huang, H.; Zhang, Q.; Zhang, P. Chirality in Metal-Based Anticancer Agents. *Dalton Trans.* **2018**, *47*, 4017−4026.

(15) Hernández-Romero, D.; Rosete-Luna, S.; López-Monteon, A.; Chávez-Piña, A.; Pérez-Hernández, N.; Marroquín-Flores, J.; Cruz-Navarro, A.; Pesado-Gómez, G.; Morales-Morales, D.; Colorado-Peralta, R. First-Row Transition Metal Compounds Containing Benzimidazole Ligands: An Overview of Their Anticancer and Antitumor Activity. *Coord. Chem. Rev.* **2021**, *439*, 213930.

(16) Guo, Z.; Sadler, P. J. Metals in Medicine. *Angew. Chem., Int. Ed.* **1999**, *38*, 1512−1531.

(17) Lengacher, R.; Marlin, A.; Śmiłowicz, D.; Boros, E. Medicinal Inorganic Chemistry-Challenges, Opportunities and Guidelines to Develop the Next Generation of Radioactive, Photoactivated and Active Site Inhibiting Metal-Based Medicines. *Chem. Soc. Rev.* **2022**, *51*, 7715−7731.

(18) Barry, N. P.; Sadler, P. J. Challenges for Metals in Medicine: How Nanotechnology May Help to Shape the Future. *ACS Nano* **2013**, *7*, 5654−5659.

(19) Lipinski, C. A.; Lombardo, F.; Dominy, B. W.; Feeney, P. J. Experimental and Computational Approaches to Estimate Solubility and Permeability in Drug Discovery and Development Settings. *Adv. Drug Delivery Rev.* **2012**, *64*, 4−17.

(20) Fricker, S. P. Metal Based Drugs: From Serendipity to Design. *Dalton Trans.* **2007**, 4903−4917.

(21) Cutillas, N.; Yellol, G. S.; de Haro, C.; Vicente, C.; Rodríguez, V.; Ruiz, J. Anticancer Cyclometalated Complexes of Platinum Group Metals and Gold. *Coord. Chem. Rev.* **2013**, *257*, 2784−2797.

(22) Albrecht, M. Cyclometalation Using D-Block Transition Metals: Fundamental Aspects and Recent Trends. *Chem. Rev.* **2010**, *110*, 576−623.

(23) Cai, J.; Yue, Y.; Rui, D.; Zhang, Y.; Liu, S.; Wu, C. Effect of Chain Length on Cytotoxicity and Endocytosis of Cationic Polymers. *Macromolecules* **2011**, *44*, 2050−2057.

(24) Gao, E.; Zhu, M.; Liu, L.; Huang, Y.; Wang, L.; Shi, C.; Zhang, W.; Sun, Y. Impact of the Carbon Chain Length of Novel Palladium (Ii) Complexes on Interaction with DNA and Cytotoxic Activity. *Inorg. Chem.* **2010**, *49*, 3261−3270.

(25) Karami, K.; Jamshidian, N.; Hajiaghasi, A.; Amirghofran, Z. BSA Nanoparticles as Controlled Release Carriers for Isophethalaldoxime Palladacycle Complex; Synthesis, Characterization, in Vitro Evaluation, Cytotoxicity and Release Kinetics Analysis. *New J. Chem.* **2020**, *44*, 4394−4405.

(26) Veeralakshmi, S.; Nehru, S.; Arunachalam, S.; Kumar, P.; Govindaraju, M. Study of Single and Double Chain Surfactant-Cobalt (III) Complexes and Their Hydrophobicity, Micelle Formation, Interaction with Serum Albumins and Antibacterial Activities. *Inorg. Chem. Front.* **2014**, *1*, 393−404.

(27) Montero, A. J.; Adams, B.; Diaz-Montero, C. M.; Glück, S. Nab-Paclitaxel in the Treatment of Metastatic Breast Cancer: A Comprehensive Review. *Expert Rev. Clin. Pharmacol.* **2011**, *4*, 329−334.

(28) Solanki, R.; Rostamabadi, H.; Patel, S.; Jafari, S. M. Anticancer Nano-Delivery Systems Based on Bovine Serum Albumin Nanoparticles: A Critical Review. *Int. J. Biol. Macromol.* **2021**, *193*, 528−540.

(29) Elsadek, B.; Kratz, F. Impact of Albumin on Drug Delivery—New Applications on the Horizon. *J. Controlled Release* **2012**, *157*, 4−28.

(30) Andersen, J. T.; Dalhus, B.ør.; Cameron, J.; Daba, M. B.; Plumridge, A.; Evans, L.; Brennan, S. O.; Gunnarsen, K. S.øe.; Bjøras, M.; Sleep, D.; Sandlie, I. Structure-Based Mutagenesis Reveals the Albumin-Binding Site of the Neonatal Fc Receptor. *Nat. Commun.* **2012**, *3*, 610.

(31) Hu, D.; Xu, H.; Xiao, B.; Li, D.; Zhou, Z.; Liu, X.; Tang, J.; Shen, Y. Albumin-Stabilized Metal-Organic Nanoparticles for Effective Delivery of Metal Complex Anticancer Drugs. *ACS Appl. Mater. Interfaces* **2018**, *10*, 34974−34982.

(32) Yardley, D. A. Nab-Paclitaxel Mechanisms of Action and Delivery. *J. Controlled Release* **2013**, *170*, 365−372.

(33) Sleep, D. Albumin and Its Application in Drug Delivery. *Expert Opin. Drug Delivery* **2015**, *12*, 793−812.

(34) Bolaños, K.; Kogan, M. J.; Araya, E. Capping Gold Nanoparticles with Albumin to Improve Their Biomedical Properties. *Int. J. Nanomedicine* **2019**, *14*, 6387.

(35) Senapati, S.; Mahanta, A. K.; Kumar, S.; Maiti, P. Controlled Drug Delivery Vehicles for Cancer Treatment and Their Performance. *Signal Transduct. Target* **2018**, *3*, 7.

(36) Desai, N.; Trieu, V.; Yao, Z.; Louie, L.; Ci, S.; Yang, A.; Tao, C.; De, T.; Beals, B.; Dykes, D.; Noker, P.; Yao, R.; Labao, E.; Hawkins, M.; Soon-Shiong, P. Soon-Shiong, P. Increased antitumor activity, intratumor paclitaxel concentrations, and endothelial cell transport of cremophor-free, albumin-bound paclitaxel, ABI-007, compared with cremophor-based paclitaxel. *Clin. Cancer Res.* **2006**, *12*, 1317−1324.

(37) Xu, N.; Yang, Y.-F.; Chen, L.; Lin, J. A Ferritin-Albumin-Cu Nanoparticle That Efficaciously Delivers Copper (II) Ions to a Tumor and Improves the Therapeutic Efficacy of Disulfiram. *ACS omega* **2020**, *5*, 10415−10422.

(38) Tiwari, R.; Viswanathan, K.; Gour, V.; Vyas, S. P.; Soni, V. Cisplatin-Loaded Albumin Nanoparticle and Study Their Internalization Effect by Using B-Cyclodextrin. *J. Recept. Signal Transduct.* **2021**, *41*, 393−400.

(39) Das, S.; Jagan, L.; Isiah, R.; Rajesh, B.; Backianathan, S.; Subhashini, J. Nanotechnology in Oncology: Characterization and in Vitro Release Kinetics of Cisplatin-Loaded Albumin Nanoparticles: Implications in Anticancer Drug Delivery. *Indian J. Pharmacol.* **2011**, *43*, 409.

(40) Zheng, Y.-R.; Suntharalingam, K.; Johnstone, T. C.; Yoo, H.; Lin, W.; Brooks, J. G.; Lippard, S. J. Pt (IV) Prodrugs Designed to Bind Non-Covalently to Human Serum Albumin for Drug Delivery. *J. Am. Chem. Soc.* **2014**, *136*, 8790−8798.

(41) Mayr, J.; Heffeter, P.; Groza, D.; Galvez, L.; Koellensperger, G.; Roller, A.; Alte, B.; Haider, M.; Berger, W.; Kowol, C. R.; Keppler, B. K. An Albumin-Based Tumor-Targeted Oxaliplatin Prodrug with Distinctly Improved Anticancer Activity In Vivo. *Chem. Sci.* **2017**, *8*, 2241−2250.

(42) Garmann, D.; Warnecke, A.; Kalayda, G. V.; Kratz, F.; Jaehde, U. Cellular Accumulation and Cytotoxicity of Macromolecular Platinum Complexes in Cisplatin-Resistant Tumor Cells. *J. Controlled Release* **2008**, *131*, 100−106.

(43) Warnecke, A.; Fichtner, I.; Garmann, D.; Jaehde, U.; Kratz, F. Synthesis and Biological Activity of Water-Soluble Maleimide Derivatives of the Anticancer Drug Carboplatin Designed as Albumin-Binding Prodrugs. *Bioconjugate Chem.* **2004**, *15*, 1349−1359.

(44) Mertens, R. T.; Gukathasan, S.; Arojojoye, A. S.; Olelewe, C.; Awuah, S. G. Next Generation Gold Drugs and Probes: Chemistry and Biomedical Applications. *Chem. Rev.* **2023**, *123*, 6612−6667.

(45) Arojojoye, A. S.; Kim, J. H.; Olelewe, C.; Parkin, S.; Awuah, S. G. Chiral Gold (III) Complexes: Speciation, in Vitro, and in Vivo Anticancer Profile. *Chem. Commun.* **2022**, *58*, 10237−10240.

(46) Lu, Y.; Ma, X.; Chang, X.; Liang, Z.; Lv, L.; Shan, M.; Lu, Q.; Wen, Z.; Gust, R.; Liu, W. Recent Development of Gold (I) and Gold (III) Complexes as Therapeutic Agents for Cancer Diseases. *Chem. Soc. Rev.* **2022**, *51*, 5518−5556.

(47) Olelewe, C.; Kim, J. H.; Ofori, S.; Mertens, R. T.; Gukathasan, S.; Awuah, S. G. Gold(III)-P-Chirogenic Complex Induces Mitochondrial Dysfunction in Triple-Negative Breast Cancer. *iScience* **2022**, *25*, 104340.

(48) Mertens, R. T.; Parkin, S.; Awuah, S. G. Cancer Cell-Selective Modulation of Mitochondrial Respiration and Metabolism by Potent Organogold(III) Dithiocarbamates. *Chem. Sci.* **2020**, *11*, 10465−10482.

(49) Bertrand, B.; Williams, M. R.; Bochmann, M. Gold (III) Complexes for Antitumor Applications: An Overview. *Chem.—Eur. J.* **2018**, *24*, 11840−11851.

(50) Fung, S. K.; Zou, T.; Cao, B.; Lee, P. Y.; Fung, Y. M. E.; Hu, D.; Lok, C. N.; Che, C. M. Cyclometalated Gold (III) Complexes Containing N-Heterocyclic Carbene Ligands Engage Multiple Anti-Cancer Molecular Targets. *Angew. Chem., Int. Ed.* **2017**, *56*, 3892−3896.

(51) Casini, A.; Hartinger, C.; Gabbiani, C.; Mini, E.; Dyson, P. J.; Keppler, B. K.; Messori, L. Gold (III) Compounds as Anticancer Agents: Relevance of Gold-Protein Interactions for Their Mechanism of Action. *J. Inorg. Biochem.* **2008**, *102*, 564−575.

(52) Arojojoye, A. S.; Olelewe, C.; Gukathasan, S.; Kim, J. H.; Vekaria, H.; Parkin, S.; Sullivan, P. G.; Awuah, S. G. Serum-Stable Gold (III) Bisphosphine Complex Induces Mild Mitochondrial Uncoupling and in Vivo Antitumor Potency in Triple Negative Breast Cancer. *J. Med. Chem.* **2023**, *66*, 7868.

(53) Celegato, M.; Fregona, D.; Mongiat, M.; Ronconi, L.; Borghese, C.; Canzonieri, V.; Casagrande, N.; Nardon, C.; Colombatti, A.; Aldinucci, D. Preclinical Activity of Multiple-Target Gold (III)-Dithiocarbamato Peptidomimetics in Prostate Cancer Cells and Xenografts. *Future Med. Chem.* **2014**, *6*, 1249−1263.

(54) Nardon, C.; Schmitt, S. M.; Yang, H.; Zuo, J.; Fregona, D.; Dou, Q. P. Gold (III)-Dithiocarbamato Peptidomimetics in the Forefront of the Targeted Anticancer Therapy: Preclinical Studies against Human Breast Neoplasia. *PLoS One* **2014**, *9*, No. e84248.

(55) Usón, R.; Vicente, J.; Cirac, J.; Chicote, M. Synthesis and Reactivity of Dibenzometallole Complexes of Gold (III) and Platinum (Ii). *J. Organomet. Chem.* **1980**, *198*, 105−112.

(56) Wu, C.-Y.; Horibe, T.; Jacobsen, C. B.; Toste, F. D. Stable Gold(III) Catalysts by Oxidative Addition of a Carbon-Carbon Bond. *Nature* **2015**, *517*, 449−454.

(57) Langer, K.; Balthasar, S.; Vogel, V.; Dinauer, N.; Von Briesen, H.; Schubert, D. Optimization of the Preparation Process for Human Serum Albumin (HSA) Nanoparticles. *Int. J. Pharm.* **2003**, *257*, 169−180.

(58) Kim, J. H.; Ofori, S.; Parkin, S.; Vekaria, H.; Sullivan, P. G.; Awuah, S. G. Anticancer Gold (III)-Bisphosphine Complex Alters the Mitochondrial Electron Transport Chain to Induce in Vivo Tumor Inhibition. *Chem. Sci.* **2021**, *12*, 7467−7479.

(59) Parkin, S.; Hope, H. Macromolecular Cryocrystallography: Cooling, Mounting, Storage and Transportation of Crystals. *J. Appl. Crystallogr.* **1998**, *31*, 945−953.

(60) Hope, H. X-Ray Crystallography - a Fast, First-Resort Analytical Tool. *Progress in Inorganic Chemistry, Vol 41* **1994**, *41*, 1−19.

(61) Bruker *Apex2*; Bruker-Axs: Madison, WI, USA, 2006.

(62) Krause, L.; Herbst-Irmer, R.; Sheldrick, G. M.; Stalke, D. Comparison of Silver and Molybdenum Microfocus X-Ray Sources for Single-Crystal Structure Determination. *J. Appl. Crystallogr.* **2015**, *48*, 3−10.

(63) Sheldrick, G. M. *Sadabs, Program for Bruker Area Detector Absorption Correction*; University of Gottingen: Gottingen, 1997.

(64) Sheldrick, G. A Short History of Shelx. *Acta Crystallogr., Sect. A* **2008**, *64*, 112−122.

(65) Sheldrick, G. M. Crystal Structure Refinement with Shelxl. *Acta Crystallogr. C Struct Chem.* **2015**, *71*, 3−8.

(66) Sheldrick, G. M. Shelxt—Integrated Space-Group and Crystal-Structure Determination. *Acta Crystallogr. A Found Adv.* **2015**, *71*, 3−8.

(67) Spek, A. L. Structure Validation in Chemical Crystallography. *Acta Crystallogr. D Biol. Crystallogr.* **2009**, *65*, 148−155.

(68) Parkin, S. Expansion of Scalar Validation Criteria to Three Dimensions: The R Tensor. Erratum. *Acta Crystallogr. A* **2000**, *56*, 317.